PCCP

Accepted Manuscript

ROYAL SOCIETY OF CHEMISTRY

www.rsc.org/pccp

Ultrafast primary processes of the stable neutral organic radical, 1,3,5-triphenylverdazyl, in liquid solution.

Christoph Weinert[1], Boris Wezisla[1], Jörg Lindner, and Peter Vöhringer*

Lehrstuhl für Molekulare Physikalische Chemie

Institut für Physikalische und Theoretische Chemie

Rheinische Friedrich-Wilhelms-Universität

Wegelerstraße 12, 53115 Bonn, Germany

p.voehringer@uni-bonn.de

Submitted to

Physical Chemistry Chemical Physics

March 03, 2015

[1]These authors contributed equally to this work

*corresponding author

Abstract. Femtosecond spectroscopy with hyperspectral white-light detection was used to elucidate the ultrafast primary processes of the thermodynamically stable organic radical, 1,3,5-triphenylverdazyl, in liquid acetonitrile solution at room temperature. The radical was excited with optical pulses having a duration of 39 fs and a center wavelength of 800 nm thereby accessing its energetically lowest electronically excited state (D_1). The apparent spectrotemporal response is understood in terms of an ultrafast primary D_1-to-D_0 internal conversion that generates the electronic ground state of the radical in a highly vibrationally excited fashion within a few hundred femtoseconds. The replenished electronic ground state subsequently undergoes vibrational cooling on a time scale of a few picoseconds. The instantaneous absorption spectra of the radical derived from the femtosecond pump-probe data are analyzed within the Sulzer-Wieland formalism for calculating the electronic spectra of "hot" polyatomic molecules. The pump-probe spectra together with transient anisotropy data in the region of the $D_0 \rightarrow D_1$ ground-state bleach gives evidence for an additional transient absorption that arises from a dark excited state, which gains oscillator strength with increasing vibrational excitation of the radical by virtue of vibronic coupling

1. Introduction

The photophysics and photochemistry of open-shell organic species with non-zero electronic spin in the condensed phase is much less understood than those of closed-shell species.[1] This is because carbon, oxygen, or nitrogen-centered radicals are generally highly reactive and their rather short ground-state lifetimes invariably preclude an in-depth spectroscopic analysis of their photoinduced processes. Therefore, most of our knowledge of the excited state dynamics of organic compounds with unpaired electrons stems from experiments conducted on gas phase samples or molecular beam ensembles.[2] In such studies, small organic radicals like ethyl, *t*-butyl, propargyl, benzyl, allyl, or methylallyl can be generated by flash photolysis

or pyrolysis of suitably labile precursors and the primary processes following electronic excitation can be recorded in a pump-probe experiment employing e.g. a multi-photon ionization/mass-spectrometric detection scheme.[2-6] A feature that appears to be common for most hydrocarbon radicals is a rapid non-radiative excited-state decay that is often followed by the unimolecular loss of a hydrogen atom from high-lying vibrational states in the electronic ground state. Conical intersections are being held responsible for the observation of ultrashort excited state lifetimes of the orders of 1 ps to 10^2 ps.[2-6] To our knowledge, nothing is known so far about the dynamics of electronically excited neutral organic radicals in liquid solutions and the dynamical interactions with a condensed-phase solvation environment.

In contrast, the dynamics of electronically excited charged radicals have been studied quite extensively. In solution, the radicals were generated *in situ* either by chemical, electrochemical, or photochemical means and conventional pump-probe or transient grating techniques were applied.[7-11] Vauthey and coworkers have exploited liquid solutions of a neutral organic precursor compound serving as an electron donor in the presence of an electron acceptor.[12-16] Optical excitation of such samples with an actinic pump pulse generates correlated radical ion pairs in their electronic ground state. A subsequent pump pulse was then used to promote the radical cation or radical anion to its electronically excited state whose fate was then followed in transient absorption through a variably delayed probe pulse. The ground-state recovery was generally found to be very efficient with excited state lifetimes ranging from several tens of picoseconds all the way down to a few tens of femtoseconds. In some instances, evidence for a photodetachment of the unpaired electron was also found.[12] The ultrafast deactivation of the radical ion's excited state is commonly rationalized with concial intersections favoring an efficient non-radiative decay and complete lack of emission similar to neutral radicals in the gas phase.

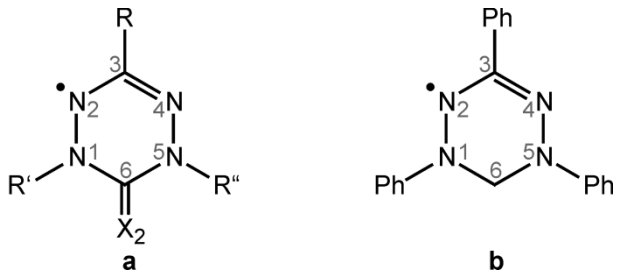

Scheme 1. a) General Lewis structure of the verdazyl class of neutral stable radicals where R, R', and R"are like or unlike alkyl or aryl substituents while X can be O, S, or H_2. b) Lewis structure of 1,3,5-triphenylverdazyl.

In this study, we explored for the first time the photoinduced primary processes of a particularly intriguing class of thermodynamically stable neutral organic radicals [17], namely verdazyls (cf. Scheme 1), and we focused particularly on the dynamics in liquid solution. These radicals were first discovered by Kuhn and Trischmann in the early 1960s.[18] Owing to an extensive delocalization of the spin density across a 1,2,4,5-tetrazine moiety, verdazyls are so stable that they can be isolated and stored for years safely just like closed-shell organic compounds. They constitute the only known class of radicals that is persistent against moisture and air without requiring bulky substituents. In liquid solution, verdazyls have a low tendency for aggregation and they are currently even considered as promising building blocks for the design of molecular magnets.[19-23]

2. Experimental

A schematic of the experimental setup is given in Figure 1. The time-resolved absorption measurements were carried out using a commercial 250 kHz Ti:sapphire regenerative amplifier (Coherent RegA 9050) driving a home-built pump-supercontinuum-probe spectrometer. The amplifier provides 800 nm pulses with a duration of 35 fs and an energy of 5.2 μJ. This output was split into two beams by a dielectric flat with a reflectivity of 30%. The

reflected beam was used to generate a single filament white-light continuum for hyperspectral probing while the transmitted beam was used for exciting the sample.

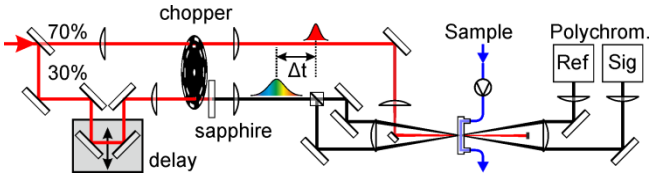

Fig. 1. Schematic of the femtosecond-pump-probe experimental setup.

A combination of a half-wave retardation plate (mica) and a Glan-Taylor polarizer was employed to control the relative polarization between the pump and the probe pulses as well as to variably adjust the pump pulse energy in the range of 80 to 800 nJ. In addition, a pair of fused silica Brewster prisms allowed for a compensation of the positive group velocity dispersion of the pump beam path. The autocorrelation function measured with a 100 µm thick type-I barium borate crystal revealed pump-pulse durations of 39 fs at the position of the sample assuming a Gaussian temporal pulse shape.

The supercontinuum probe pulses were generated by focusing the 30%-beam of the amplifier's output into a 1 mm thick sapphire substrate using a 50 mm focal length lens. The position of the sapphire plate within the focal spot was varied until a white beam with a Gaussian spatial profile was emitted from a single stable filament. A 25 mm focal length achromat was used to collimate the supercontinuum beam, which was subsequently spectrally flattened with a suitable set of KG filters (Schott). The fundamental 800 nm portion of its spectrum was suppressed by a short-pass filter (Edmund Optics short pass 750 nm, OD4).

The white light beam was then split into two almost equally intense beams using a beam splitter cube (Edmund Optics, material N-BK7, thickness 5 mm) to generate a probe and a reference beam for frequency-resolved hyperspectral detection of the third-order nonlinear-optical response of the sample. The probe and reference beams were then focused with an

achromat (f = +100 mm) into the sample, where they intersected at an angle of 10°. The pump pulses were spatially overlapped with the probe and reference pulses at their bisector using a fused silica lens (f = +200 mm). The diameter of the white-light beams inside the sample varied between 15 and 40 μm depending upon the wavelength while that of the pump beam was roughly four times larger. The optical path lengths of the three beams were chosen such that the reference pulses always preceded the pump and probe pulses regardless of the pump-probe time delay. The latter was controlled by sending the probe pulses through an optical delay line whose length was controlled by a motorized translation stage (Melles Griot, Nanomover).

The spectral intensity distribution of the signal and reference beams, I and I_{ref}, were measured independently using two identical polychromators each of which consisting of a 0.25 m monochromator (Bausch & Lomb, 33-86-75) and a NMOS linear image sensor (Hamamatsu, S3901-Q, 512 pixels). Special care was taken to match the spectral responses of both spectrometers upon exposure to the white light beams. The video signals of the two arrays were digitized with a simultaneous A/D data acquisition card (Data Translation, DT 9826) at a frequency of 1.3 kHz thereby allowing the polychromators to integrate over ~ 200 pulses. Pump and white light beams were blocked and unblocked in a 90°-phase-shifted pattern at a rate of 109 Hz, thereby allowing for the recording of the two video signals, I and I_{ref}, under the following exposure conditions: (1) probe, reference and pump beams are all unblocked; (2) probe and reference beams are unblocked and the pump beam is blocked; (3) probe and reference beams are blocked and the pump beam is unblocked; and (4) all beams are blocked. From these four conditions, the conventional pump-induced differential optical density corrected for pump scatter and electronic background was computed as from [24]:

$$\Delta OD = \log\left(\frac{I_{ref}^{(1)} - I_{ref}^{(3)}}{I^{(1)} - I^{(1)}}\right) - \log\left(\frac{I_{ref}^{(2)} - I_{ref}^{(4)}}{I^{(2)} - I^{(4)}}\right) \quad (1)$$

where the number in parenthesis denotes the exposure condition. At each pump-probe delay, the signal was averaged over 250 measurement cycles or equivalently, over roughly 50.000 laser shots, which resulted in a signal-to-noise ratio for ΔOD of ~150.

The white-light continuum accumulated a significant positive group velocity dispersion as it traveled through the optical components of the probe and reference beam paths; thus, causing a probe wavelength-dependent temporal shift of the third-order response that required a careful correction. To this end, the impulsive nonresonant pump-probe response of the pure solvent was measured and a chirp correction was carried out similar to that described by Kovalenko and Ernsting.[25]

The sample consisted of a 1 mM solution of 1,3,5-triphenylverdazyl in acetonitrile with an optical density of 0.15 at 800 nm. The compound was synthesized as described by Kuhn and Trischmann [18] and its purity has been verified by mass spectrometry. Moreover, 1,3,5-triphenylverdazylium tetrafluoroborate was synthesized according to Ref. [26]. Acetonitrile (Sigma-Aldrich, Chromasolv) was used as purchased without further purification. The sample solution was circulated through a fused silica flow cell (Hellma, optical path length of 1 mm) at a flow rate of 5 L/min thereby exchanging the pump focal volume after roughly five laser shots. No artefacts from thermal lensing or local heating effects were observed. Linear absorption spectra were measured with a commercial UV/VIS spectro-photometer (Shimadzu UV-160).

3. Computational

Electronic structure calculations within the framework of the density functional theory (DFT) were performed with the ORCA program package [27] using the B3LYP functional [28-30] and Ahlrichs' triple-zeta valence basis set, def2-TZVPP.[31-32] Whenever possible the RIJCOSX

approximation [33-34] was invoked to speed up the calculations without considerable loss of accuracy. Solvent effects were accounted for by employing the conductor-like screening model (COSMO).[35-36]

Geometry optimizations were considered to be converged if the following three convergence criteria were achieved at the same time: energy < $1 \cdot 10^{-6}$ Eh, root mean square of the displacements < $1 \cdot 10^{-4}$ bohr, and root mean square of the gradient < $3 \cdot 10^{-5}$ Eh/bohr. Stationary points were checked to be true local minima of the potential energy surface (PES) by performing Hessian calculations. Relaxed PES scans along various internal coordinates were also carried out and utilized the exact same model chemistry and convergence criteria as the single molecular structure optimizations.

Time-dependent DFT (TD-DFT) calculations [37-38]were performed within the Tamm-Duncoff approximation [39] to obtain the lowest 40 roots for stationary points or the lowest 20 roots when PES scans were carried out. The RIJCOSX approximation is also applicable to excited state calculations and was used throughout.[40-41] The integration grid for TD-DFT calculations was increased beyond the program standard to reduce numerical noise. For comparison, TD-DFT absorption spectra for the geometrically relaxed ground state were also calculated with the gradient-corrected pure BLYP functional [28, 30] and the double-hybrid B2PLYP functional.[42-43] The same basis sets were used as for the geometry optimization (*vide supra*).

Theoretical UV/Vis spectra were generated by a superposition of Gaussian lineshape functions, each of which centered at the predicted transition energy and scaled such that their integral corresponds to the predicted oscillator strength. The full width at half maximum (FWHM) parameter was set to 3750 cm^{-1}. In addition, the theoretical spectrum was subjected to the empirical UV correction by shifting it along the energy axis so as to obtain the best agreement between the measured and the calculated spectra in the region of the two

energetically lowest transitions. The used UV correction parameters were +750 cm^{-1} (+0.093 eV) for B3LYP, –1250 cm^{-1} (–0.155 eV) for B2PLYP and +5750 cm^{-1} (+0.713 eV) for BLYP.

4. Results and Discussion

4.1 Linear Spectroscopy

The electronic absorption spectrum of 1,3,5-triphenylverdazyl radicals (3,4-Dihydro-2,4,6-triphenyl-Stetrazin-1(2H)-yl) in acetonitrile solution at room temperature is shown in Figure 2a. In the visible-to-near-UV spectral region, it consists of two very broad and unstructured bands that are centered at 13970 cm^{-1} (corresponding to a peak wavelength of 716 nm) and 24940 cm^{-1} (401 nm), respectively. These two features are responsible for the characteristic green color of the radical, hence the name verdazyl derived from the latin word viridis (green). The low-energy band has a peak extinction coefficient of ~3800 L mol^{-1} cm^{-1}, it is slightly asymmetric in shape and has an enormous full spectral width at half maximum (FWHM) of almost 3000 cm^{-1}. Its steeper edge extends well into the near-infrared region beyond 12500 cm^{-1}, which corresponds to the photon energy of the 800 nm excitation pulses used in the femtosecond experiments described here. At the pump-photon energy, the compound still features an appreciable extinction coefficient of ~1400 L mol^{-1} cm^{-1}.

The second band peaks at 24940 cm^{-1} (401 nm) and is characterized by a noticeably flattened maximum. With a FWHM of almost 5700 cm^{-1}, it is spectrally even broader than the low-energy band. It has a peak extinction coefficient of ~7300 L mol^{-1} cm^{-1} and is thus almost twice as intense as the near-infrared-to-Vis resonance. The ultraviolet part of the spectrum consists essentially of a very strong resonance peaking at 36100 cm^{-1} (277 nm, ~20500 L

mol^{-1} cm^{-1}) with two minor side bands centered at 31750 cm^{-1} (315 nm, ~12200 L mol^{-1} cm^{-1}) and 40980 cm^{-1} (244 nm, ~12100 L mol^{-1} cm^{-1}), respectively.

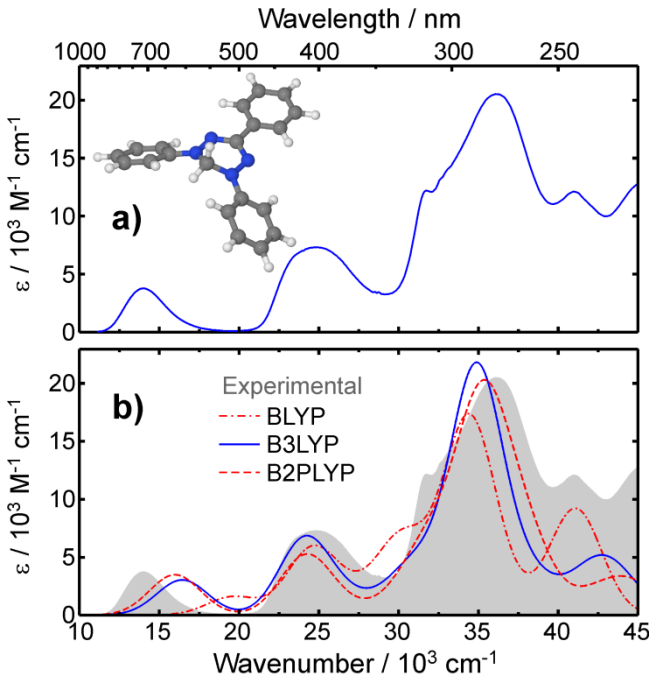

Fig. 2. a) Linear UV/Vis absorption spectrum of 1,3,5-triphenylverdazyl in acetonitrile solution at room temperature. The inset shows the DFT-optimized structure of the radical. b) Electronic spectrum of 1,3,5-triphenylverdazyl from TD-DFT calulations obtained for three different functionals.

4.2 Molecular and Electronic Structure

The DFT-optimized geometry of 1,3,5-triphenylverdazyl has C_S-symmetry and is depicted in the inset of Figure 2a. It can be seen that the central tetrazine ring adopts a half-boat structure with the two carbon atoms being located slightly above the plane formed by the four nitrogen atoms. The ring puckering angle involving the sp^3-hybridized methylenic carbon atom, C-6 (cf. Scheme 1), amounts to 42.5° while the sp^2-hybridized carbon atom, C-3, is nearly coplanar with the four nitrogens (puckering angle 5.8°). Except for C-6 and the hydrogens, all other atoms are sp^2-hybridized and belong to a single delocalized π-system. As a result, the

phenyl ring attached to C-3 is almost perfectly coplanar with the four N-atoms. Due to the ring puckering, the other two phenyl rings are slightly twisted away from the plane defined by the tetrazine's N-atoms thus, forming a butterfly fold with an angle between the two phenyl ring normals of 58.2° and an angle between the two C-N-bonds of 121°. According to our calculations, the structure shown in Figure 2a is the only stable conformation with a closed tetrazine ring. A normal mode analysis identifies the linear combinations of the three local phenyl torsional degrees of freedom as the vibrations of the radical that have the lowest frequencies.

The unpaired electron is extensively delocalized across this π-system, and according to a Löwdin spin population analysis [44-45], a fraction of 52% of the total spin density is evenly split over the N-2 and N-4 atoms of the tetrazine moiety while another fraction of 30% is spread equally over N-1 and N5. The remaining 18% of the total spin density is delocalized over the C-atoms with the majority being distributed over the ortho- and para-positioned carbons of the N-bound phenyl rings. While the DFT-optimized geometry is in good agreement with the x-ray crystal structure [46-47] and earlier low-level ab initio calculations [48], the theoretical spin density is corroborated by electron paramagnetic resonance data.[49] Both, the extensive delocalization of the unpaired electron and the conformational stability of the electronic ground state rationalize the remarkably high stability of this open-shell species.

The UV/Vis spectra obtained from the TD-DFT-calculations are shown in Figure 2b. It can be seen that the spectrum obtained from the pure BLYP-functional deviates significantly from the experimental spectrum. In particular, the energetic splitting and the amplitude ratio between the two lowest resonances are unsatisfactory. However, an inclusion of exact exchange by using the hybrid B3LYP-functional improves the agreement between experimental and theoretical spectra significantly. Yet, mixing in a second-order pertubative correlation through the double-hybrid density functional, B2PLYP, does not enhance the

agreement between experiment and theory to such an extent that the greatly increased computational cost would be justified. Therefore, only theoretical results obtained with B3LYP will be discussed from hereon.

The overall shape of the spectrum as well as the predicted band positions are reasonably well reproduced with the TD-DFT method. The lowest absorption band is predicted at 16450 cm^{-1} and only consists of a transition to a single state, which will be denoted D_1. The second band is predicted at 24100 cm^{-1} and belongs primarily to a transition into a state denoted D_2. A second, weaker transition into a state D_5 at 26810 cm^{-1} leads to the asymmetric band shape. The two intermediate states at 25580 cm^{-1} (D_3) and 26115 cm^{-1} (D_4) are spectroscopically dark, i.e. their transition dipoles from D_0 are vanishingly small. The general shape of the UV part of the spectrum is also represented reasonably well. Overall, it appears as if DFT/TD-DFT (B3LYP) is a reliable level of theory for characterizing the electronic structure of the radical including its excited states that are accessed in the near-infrared-to-near-UV part of the spectrum.

The TD-DFT calculations suggests that the D_1 and D_2 state arise from mixed single-electron promotions from the highest occupied molecular orbital (HOMO) to the singly occupied molecular orbital (SOMO) and from the SOMO to the lowest unoccupied molecular orbital (LUMO). Whereas D_1 is predominantly HOMO-to-SOMO in character (88%), D_2 is primarily SOMO-to-LUMO in nature (83%). Isosurfaces of the difference densities (i.e. electron density of the excited state minus that of the ground state) are reproduced in Figure 3 for the two energetically lowest electronic transitions. It can be seen that the $D_0 \rightarrow D_1$ transition leads mostly to a charge redistribution within the central tetrazine ring with only very minor involvement of the phenyl rings.

In stark contrast, $D_0 \rightarrow D_2$ results in a net charge-transfer from the tetrazin moiety to the penyl ring bound to C-3. Interestingly, the negative lobes of the $D_0 \rightarrow D_2$ isosurface closely

resembles the ground-state spin density of the radical thus implying that the unpaired electron is indeed removed from the SOMO and transferred completely into an orbital, which appears to be essentially a π* antibonding orbital of the phenyl ring. As described previously and in line with this charge-transfer notion of the $D_0 \rightarrow D_2$ transition, a functionalization of the 3-positioned phenyl ring in its ortho and para positions with electron donating and electron withdrawing groups leads to pronounced spectral shifts of the 400 nm band.[23]

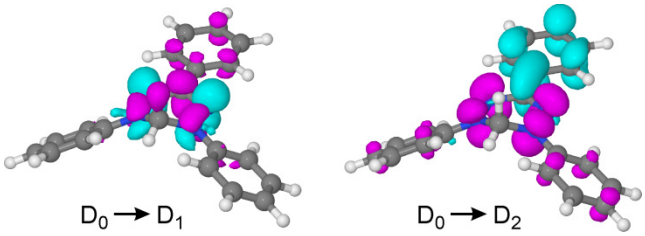

Fig. 3. Electron difference densities associated with the two energetically lowest optical transitions. An increase (decrease) of the transition-induced electron density is color-coded in cyan (magenta).

4.3 Femtosecond Spectroscopy

A contour representation of the femtosecond pump-probe data following 39 fs, 800 nm excitation of 1,3,5-triphenylverdazyl in acetonitrile solution at room temperature are displayed in Figure 4a. The vertical axis represents the probe wavelength while the horizontal axis represents the pump-probe time delay. It can be seen, that immediately after optical excitation of the radical, the $D_0 \rightarrow D_1$ transition near 720 nm is bleached. Concurrently, a very strong induced absorption is detected for probe wavelengths shorter than 650 nm. Furthermore, it can be recognized that absorption and bleaching signals decay simultaneously on an ultrafast time scales of less than 10 ps. Representative cuts through the data along the probe wavelength for various time delays yield time-dependent pump-induced differential transmission spectra. At the earliest delays, the induced absorption peaks at 490 nm, but it

slightly moves with increasing time delay to shorter wavelengths. A similar blueshift, albeit not quite as pronounced, can be observed for the ground-state bleach.

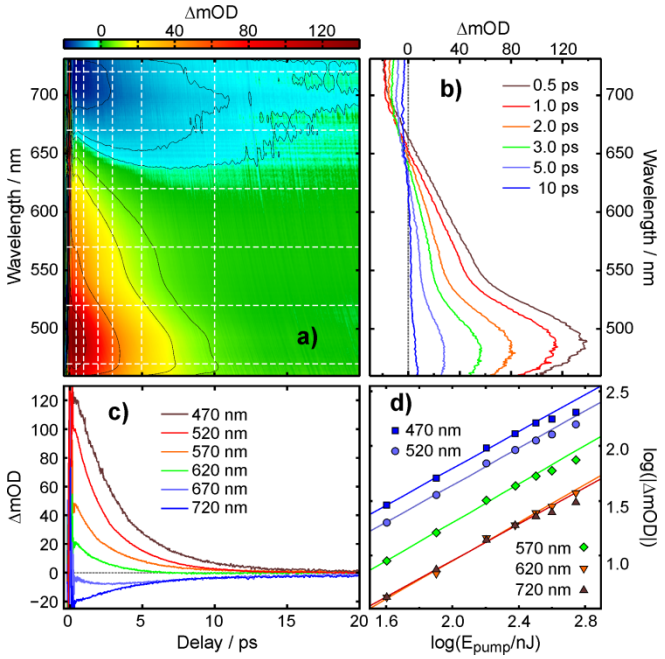

Fig. 4. a) Femtosecond pump-probe data of 1,3,5-triphenylverdazyl in acetonitrile solution at room temperature following 39 fs, 800 nm excitation. b) Representative pump-induced differential transmission spectra for various pump-probe delay. c) Representative time-resolved traces for various probe wavelengths. d) Dependence of the amplitude of the pump-probe signal on the energy of the pump pulse.

The dynamic spectral shifting is clearly evidenced by the zero-crossing wavelength where the signal reverses its sign. At a delay of 500 fs, the signal vanishes at 664 nm whereas at a delay of 10 ps, the signal becomes zero at 622 nm. Most importantly, the magnitude of the induced absorption is almost a factor of 6 larger than the bleach of the $D_0 \rightarrow D_1$ transition. This pronounced bleach deficiency is actually quite remarkable as the $D_0 \rightarrow D_1$ transition usually dominates the femtosecond pump-probe response in the spectral vicinity of the pump pulse.[50]

This finding is highly suggestive of an additional absorptive electronic transition that compensates the signal arising from the depleted electronic ground-state (*vide infra*).

Representative cuts through the pump-probe data along the delay axis for various probe wavelengths yield time-resolved kinetic traces, from which one can extract more detailed information about the nature of the dynamics. Firstly, a pronounced induction period can be noticed, lasting for about 500 fs to almost 2 ps depending upon the probe wavelength, during which the signals (bleach and absorption) barely decay or even grow in (see for example the bleaching signal at 670 nm). Once the induction period is over, the signals continuously decrease with time and their tails can be fitted by single-exponential decays. The corresponding time constants vary between 3.2 ps at 460 nm to 1.8 ps at 620 nm. However, it must be emphasized that throughout the entire probe region, single-exponential fits provide only a very crude approximation for the signal decays and in general, more exponential components are required to reproduce the data quantitatively. Regardless of the fitting function, it can be concluded that the electronic ground state is replenished and fully relaxed within less than 20 ps. This is because within the signal-to-noise ratio, all pump-induced signals have disappeared almost completely within this time window.

Finally, before closing this section, it must be stressed that an accidental degeneracy arises in the electronic structure of the verdazyl radical that is easily seen by inspecting once again the linear UV/Vis absorption spectrum (cf. Figure 2a). It turns out that within the spectral bandwidths of the corresponding resonances, the energy gap, $D_0 \rightarrow D_1$, is approximately equal to the energy gap, $D_1 \rightarrow D_2$, namely ~13000 cm^{-1}). Therefore, it is quite feasible that the D_2 state is also accessed by the pump pulse through a 2-photon-excitation process. To disclose the number of photons involved in the interaction of the pump pulse with the radical, the magnitude of the pump-induced signal was recorded at a delay of 500 fs for various probe wavelengths. The differential optical densities from these measurements as a function of the

pump-pulse energy are depicted in Figure 4d in a double-logarithmic representation. It can be seen that for a given probe wavelength the data strictly follow a straight line with a slope of 1 thereby strongly suggesting that the radical is indeed prepared in its D_1 state through a single-photon excitation scheme.

4.4 Vibrational Relaxation

The previous section has demonstrated unambiguously that in response to an 800 nm excitation, the radical returns to its equilibrated electronic ground state within ~20 ps. Apparently, the radical undergoes an ultrafast primary $D_1 \rightarrow D_0$ non-radiative transition thereby initially populating energetically high-lying vibrational states of D_0. Without knowing at this stage the nuclear degrees of freedom which can bring about such an ultrafast non-adiabtic transition, it seems intuitive to infer that the apparent spectro-temporal response is primarily caused by the ensuing vibrational energy relaxation (i.e. intramolecular vibrational redistribution and vibrational energy transfer of the excess energy into the solvent) in the electronic ground state. The induction period that was observed in the femtosecond pump-probe data at the earliest delays might be taken as a spectroscopic fingerprint of the preceding electronically non-adiabatic transition and it provides an upper limit for the lifetime of the D_1 state of about 500 fs. An interpretation of the spectro-temporal response that invokes the vibrationally relaxing electronic ground state as the only detectable species for delays in excess of 500 fs is further supported by the inability of a single-exponential decay to quatitatively fit the kinetic traces and by the wavelength dependence of the exponential time constants. Moreover, all our efforts at measuring the stationary fluorescence spectrum of verdazyl radicals in acetonitrile solution remained fruitless indicating that the fluorescence quantum yield is indeed very small. In addition, we attempted to time-resolve the spontaneous emission from the electronically excited state using time-correlated single photon counting to obtain a direct measure of its lifetime. Yet, these experiments were also unsuccessful thereby

lending additional support for an ultrafast (i.e. sub-picosecond) non-radiative decay of the D_1-state of verdazyl.

To put this scenario onto a more quantitative basis, the pump-probe data were simulated using the well-known Sulzer-Wieland formalism for computing the electronic absorption spectra of vibrationally "hot" polyatomic molecules.[51-53] Within this formalism, the extinction coefficient of the molecule as a function of temperature, T, can be expressed as

$$\epsilon(\tilde{\nu}, T) = \epsilon_0^m \frac{\tilde{\nu}}{\tilde{\nu}_{0,eff}} \left\{ \tanh\left(\frac{\Theta_{vib}}{2T}\right) \right\}^{1/2} \exp\left[-\tanh\left(\frac{\Theta_{vib}}{2T}\right) \cdot \left(\frac{\tilde{\nu} - \tilde{\nu}_{eff}}{\Delta\tilde{\nu}_0}\right)^2 \right] \quad (2)$$

where $\Theta_{vib} = hc\tilde{\nu}_{vib}/k_B$ is the characteristic temperature of the excited mode with harmonic wavenumber, $\tilde{\nu}_{vib}$, h is Planck's constant, c is the speed of light, and k_B is Boltzmann's constant. Furthermore, the quantities, ϵ_0^m and $\Delta\tilde{\nu}_0$, denote the peak extinction coefficient and the spectral width of the absorption band at some reference temperature (e.g. 0 K). The effective spectral position of the absorption band is given by its spectral position at 0 K, $\tilde{\nu}_0$, and includes an instantaneous red shift that arises from the average vibrational energy in the excited mode, i.e.

$$\tilde{\nu}_{eff} = \tilde{\nu}_0 - \tilde{\nu}_{vib}[\exp(\Theta_{vib}/T) - 1]^{-1} \quad (3)$$

thereby introducing a slight temperature-dependent shift of the electronic resonance. Thus, the influence of the vibrational excitation of a polyatomic molecule on the spectral shape of its electronic resonances is reduced to the coupling of a single "effective" vibrational degree of freedom to the electronic transition dipole. Indeed, the analytic expressions (1) and (2) were originally derived for a diatomic molecule using a harmonic potential for its electronic ground state and the well-known reflection principle for approximating the Franck-Condon factors of bound-to-continuum transitions.

In the case of 1,3,5-triphenylverdazyl, two such transitions have to be considered corresponding to the $D_0 \rightarrow D_1$ transition peaking at 716 nm and the $D_0 \rightarrow D_2$ transition

peaking at 401 nm. Each of these bands has its own unique parameter set consisting of ϵ_0^m, $\Delta\tilde{\nu}_0^*$, and $\tilde{\nu}_0$, but to minimize the number of free floating parameters, they share a common value for Θ_{vib} representing the frequency of the excited vibrational mode. Altogether, this results in seven fitting parameters (two peak extinction coefficients, two spectral widths, two spectral positions, and one characteristic temperature), which were determined first by obtaining a reasonable representation of the linear absorption spectrum of the radical as shown in Figure 5a. The Sulzer-Wieland formalism is of course unable to reproduce the flat-top shape of the 400 nm-resonance but the spectral positions and bandwidths are reasonably well approximated for our current purposes. The simulation parameters are compiled in Table I.

Table 1. Sulzer-Wieland parameters.

Parameter	720-nm band	401-nm band
$\Theta_{\mathrm{vib}}/\mathrm{K}$	2250	
$\tilde{\nu}_0/\mathrm{cm}^{-1}$	13950	24700
$\Delta\tilde{\nu}_0/\mathrm{cm}^{-1}$	1730	2710
$\epsilon_0^{\mathrm{m}}/\ (\mathrm{L\,mol}^{-1}\mathrm{cm}^{-1})$	3800	7900

Figure 5b displays several "hot" absorption spectra for various temperatures from room temperature all the way up to 3500 K. The two absorption bands exhibit an enormous broadening and energetic upshift with increasing temperature as expected. Theoretical thermal difference spectra can now be calculated by simply subtracting the room temperature data from the spectra at elevated temperatures as shown in Figure 5c. Apparently, raising the temperature leads to two negative features that spectrally coincide with the two electronic

resonances. In other words, the $D_0 \rightarrow D_1$ and $D_0 \rightarrow D_2$ bands are bleached upon heating of the radical. Moreover, the two bleaching bands are separated by a strong induced absorption that peaks around 490 nm, that connects the high-lying vibrational manifold of the electronic ground state, $D_{0,hot}$, with the D_2 state. The complementary $D_{0,hot} \rightarrow D_1$ transitions give rise to a slightly weaker induced absorption reaching out toward the near-infrared spectral region. The pronounced absorptive signal in the visible is indeed highly reminiscent of the induced absorption observed in the femtosecond pump-probe data and lends further credence to our notion that the dynamics of vibrational cooling are responsible for the spectro-temporal evolution of the radical on a ~20 ps time scale.

Before attempting to fit the experimental pump-probe spectra more quantitatively with the Sulzer-Wieland formalism, it is important to recall the underlying notions in such a simulation. Firstly, one assumes that the excitation pulse and the ensuing ultrafast internal conversion generates the "hot" electronic ground state in a quasi-instant fashion. In other words, the excess energy relative to the thermalized D_0-state that is delivered by the pump photon at $t = 0$ is canonically redistributed over all the intramolecular degrees of freedom of the radical that can couple to the two ($D_0 \rightarrow D_1$ and $D_0 \rightarrow D_2$) electronic transition dipoles. Energy can flow away from these Franck-Condon active modes either by intramolecular vibrational redistribution (IVR) to other "dark" modes of the radical or it can be dissipated into the solvent by means of intermolecular vibrational energy transfer (VET).

Secondly, and just as importantly, during the course of relaxation, the energy redistribution within the subset of Franck-Condon active modes must be much faster than energy withdrawal from these modes such that at any instant in time, a temperature suffices to describe the internal energy of the solute. Figure 6a shows a set of experimental pump-probe spectra of triphenylverdazyl for six different but representative time delays. For direct

comparison, Figure 6b shows a complementary simulation for the very same time delays using a simple single-exponential decay of the temperature according to

$$T(t) = [T(0) - T(\infty)]\ \exp(-t/\tau_{cool}) + T(\infty) \quad (3)$$

where T(0) and T(∞) are the initial and final temperatures, and τ_{cool} is the cooling time.

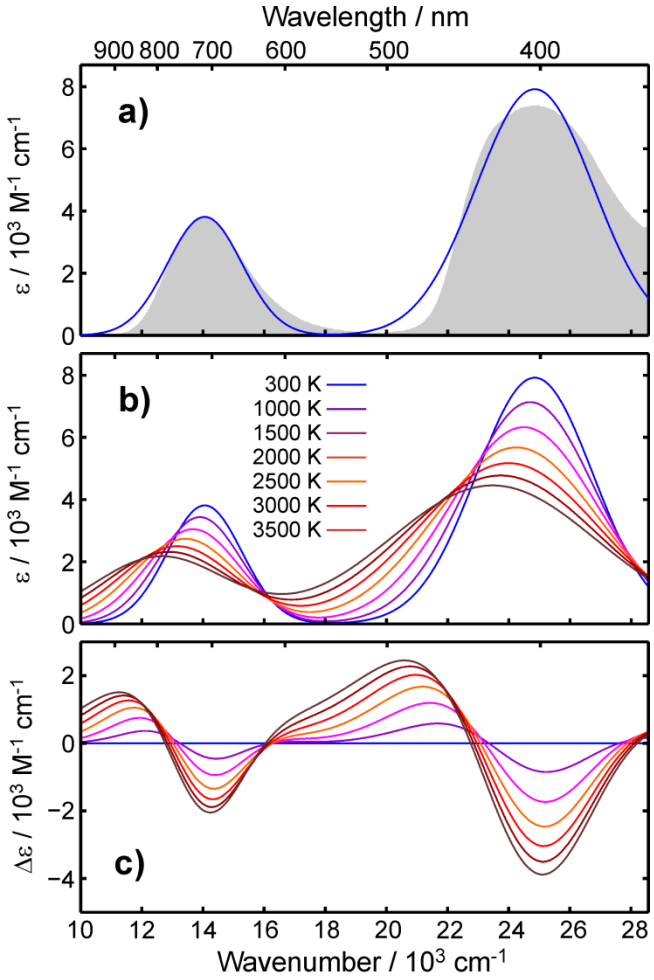

Fig. 5. Simulation of temperature-dependent linear absorption and induced (thermal difference) absorption spectra of 1,3,5-triphenylverdazyl radicals using the Sulzer-Wieland formalism. a) Comparison between the experimental and the simulated spectra at room temperature. b) Representative absorption spectra for various temperatures. c) Representative thermal difference spectra for various temperatures.

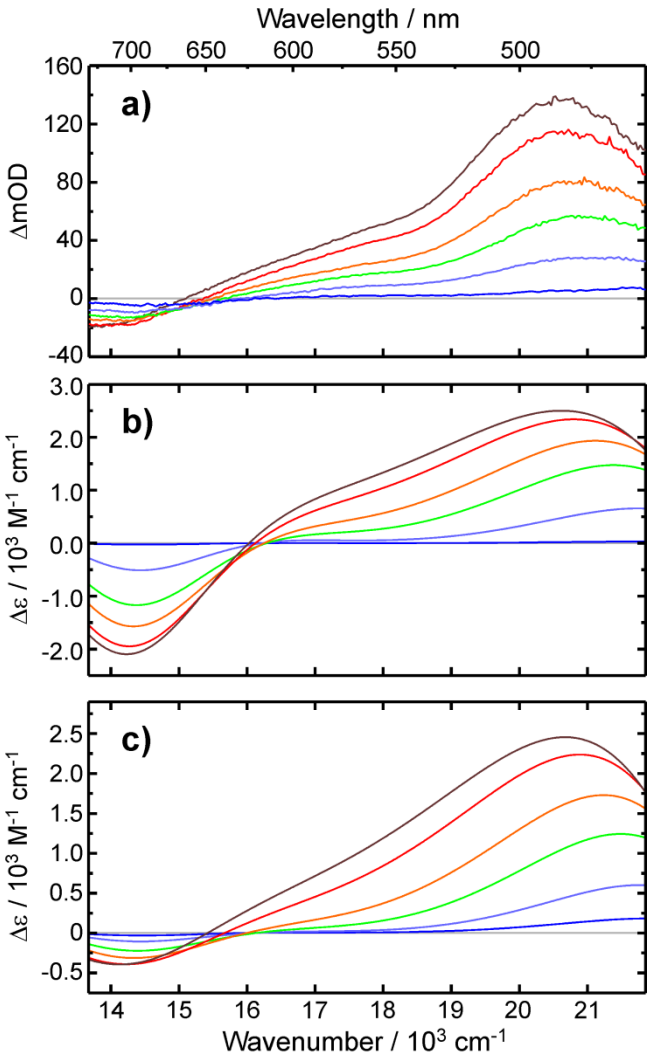

Fig. 6. a) Pump-induced differential absorbance spectra of 1,3,5-triphenylverdazyl for various pump-probe delays. b) Simulation of the spectra using the Sulzer-Wieland formalism. c) As in b) but with the $D_0 \rightarrow D_1$ transition scaled. The delay times are 500 fs (brown), 1 ps (red), 2 ps (orange), 3 ps (green), 5 ps (light blue), and 10 ps (dark blue).

The triphenylverdayzyl has 41 atoms and accordingly, it has 117 vibrational degrees of freedom whose harmonic frequencies are readily derived from the DFT-optimized structure. The 800 nm pump photon carries an energy of 12500 cm^{-1}, which would correspond to a temperature of 545 K if it were redistributed over all these vibrational modes of the radical in a canonical fashion. In the hypothetical limit of a single Franck-Condon active mode having a

value of Θ_{vib} as listed in Table 1, the initial temperature would adopt a maximum value of ~19100 K. For the simulations in Figure 6b, an initial temperature, T(0), of 4300 K was used together with a cooling time, τ_{cool}, of 3.0 ps and a final temperature, T(∞), of 300 K. It can be seen that the simulations are able to reproduce the spectral position of the induced absorption in the visible rather well, but its decay appears to be too slow during the early phase of the relaxation and too fast during the later stages.

The most important shortcoming of the simulation is however its inability to reproduce the bleach deficiency that was already noted in the previous section. From Figure 6a, an experimental absorption-to-bleach peak ratio of roughly 5.6 to 1 can be extracted. In contrast, the predicted absorption amplitude in the visible (around 20000 cm^{-1}) and the predicted bleaching amplitude in the near-IR (around 14000 cm^{-1}) are approximately equal (1.15 to 1).

Therefore, to improve the simulations, we scaled down phenomenologically the absorption cross section of the $D_0 \rightarrow D_1$ transition by a factor of 0.2. Moreover, a double-exponential function according to

$$T(t) = T(\infty) + [T(0) - T(\infty)]\{f \cdot \exp(-t/\tau_{cool,1}) + (1-f) \cdot \exp(-t/\tau_{cool,2})\} \quad (4)$$

was used to better reproduce the temperoral behavior of all spectral features. The initial and final temperatures were adopted from the previous fit. The two cooling times, $\tau_{cool,1}$ and $\tau_{cool,2}$, were set to 2.0 ps and 20 ps, respectively; and the fractional parameter, f, was adjusted to 0.86. The resultant pump-probe spectra are displayed in Figure 6c. Indeed, the scaling procedure together with the bi-exponential cooling model results in a much better agreement between experiment and simulation. Yet, the following questions immediately arise. What are the origins for the two exponential components comprising the temperature decay and what is the physico-chemical justification for scaling down the $D_0 \rightarrow D_1$ transition?

The fit parameters suggest that the faster of the two exponential components has a magnitude of 3450 K while that of the slower component is 550 K. Interestingly, the latter value matches nicely the temperature that is expected upon canonical redistribution of the photon energy over all 3N-6 vibrations of the radical. This agreement in turn strongly implies that the slower exponential decay with a time constant of 20 ps is associated with energy dissipation; that is, the transfer of vibrational energy into the liquid solvent surrounding the radical. Accordingly, the faster of the two exponentials with a time constant of 2.0 ps must then be the vibrational energy flow from the Franck-Condon active modes into the dark modes of the solute. Such an assignment is indeed quite consistent with the commonly accepted view that intramolecular vibrational redistribution is generally faster than intermoleculer vibrational energy transfer in particular, in the case of nonpolar solutes such as verdazyls that are weakly coupled to their environment.

4.5 Electron Detachment

We finally turn our attention to the bleach deficiency in the region of the $D_0 \rightarrow D_1$ transition and the rationale for phenomenologically scaling its absorption cross section. An artifically diminished magnitude of the ground-state bleach can only occur if the negative signal is partially obscured by additional absorptive signals having opposite sign. It turns out that solvated electrons in liquid acetonitrile absorb very strongly in the near-infrared. According to Doan and Schwartz, the solvated electron resonance is maximal at 1450 nm with a peak extinction coefficient in excess of $2 \cdot 10^4$ L mol^{-1} cm^{-1}.[54-55] At 720 nm, where the peak of the $D_0 \rightarrow D_1$ band of verdazyl is located, the electron's extinction coefficient still amounts to 2000 L mol^{-1} cm^{-1} and is thus only a factor of 1.5 smaller than that of the radical. This would explain why a net –albeit weak– bleach is detected.

If solvated electrons were indeed responsible for the diminished bleaching amplitude, we must clarify the mechanism that can actually lead to the generation of solvated electrons.

Since acetonitrile is transparent at the pump wavelength, it must be concluded that solvated electrons can only be generated from the solvent through a multi-photon ionization process.[56-59] Yet, the pump-probe signals scale linearly with the pump intensity as was discussed in the context of Figure 4d. The only mechanism, which can lead to solvated electrons in a one-photon excitation scheme, is the photodetachment of an electron from the triphenylverdazyl radical, V, itself, i.e.

$$V + h\nu_{800\,nm} \rightarrow V^+ + e^-_{solv}\,. \qquad (5)$$

This detachment is formally equivalent to the well-known charge-transfer-to-solvent excitation [60] of an anion except that here, the solute is an open-shell neutral species and the molecular fragment accompanying the electron is a closed-shell cation; namely, the triphenylverdazylium cation, V^+.[61-63]

Because photodetached electrons are inevitably escorted by the cation, its absorption spectrum also needs to be taken into account. The latter is characterized by a very strong absorption band in the visible spectral region that is maximal at 18690 cm^{-1} (535 nm) and has a FWHM of more than 4600 cm^{-1}. Thus, the cation absorption covers the entire spectral gap between the $D_0 \rightarrow D_1$ and $D_0 \rightarrow D_2$ transitions. Its peak extinction coefficient (9100 L mol^{-1} cm^{-1}) exceeds those of the radical's near-IR and near-UV bands. The UV/Vis absorption spectra of all three species involved in a possible photodetachment process are displayed in Figure 7a. From these data, a pump-probe spectrum can be calculated by subtracting the radical's absorption from the sum of the spectra of the cation and the electron. Surprisingly, even without taking internal conversion and hot-ground state formation into consideration, such a photodetachment spectrum is indeed reminiscent of the experimental pump-probe data with a peak-to-peak ratio of absorption and bleach of about 6:1.

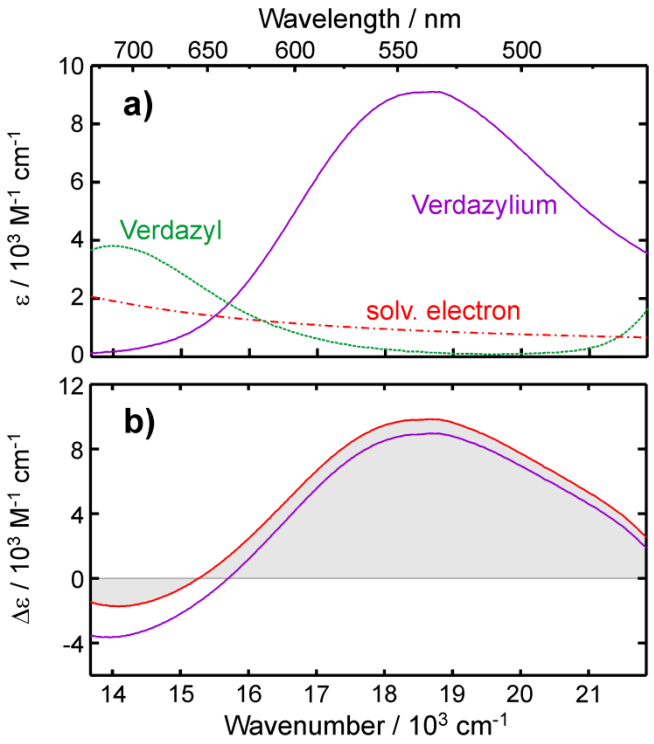

Fig. 7. a) Comparison of the UV/Vis absorption spectra of triphenylverdazylium cations, triphenylverdazyl radicals, and solvated electrons in acetonitrile at room temperature. The solvated electron's spectrum is taken from Ref. [54]. b) Difference spectrum calculated from the data in a). The gray shaded spectrum in b) is obtained when the solvated electron's absorption is taken into account. The solid curve is the spectrum where the solvated electron's contribution is neglected.

However, it has to be emphasized that solvated electrons and verdazylium cations are destined to suffer from geminate recombination [56-59] thereby most likely reforming the radical's ground electronic state. Consequently, the positive and negative features in Figure 7b will ultimately decay in concert so as to form an isosbestic point at their zero-crossing probe wavelength of 656 nm. A true isosbestic point however, cannot be observed in the experimental data. Moreover, the induced absorption in the photodetachment spectrum is maximal where the verdazylium cation absorbs, i.e. at 535 nm, whereas the induced absorption in the experimental spectra peaks at 485 nm. Moreover, it must also be stressed

that verdazylium cations have neither been observed in previous studies of the stationary photochemistry that can induced upon continuous irradiation of the near-IR band of verdazyl radicals. A net photooxidation of the radical with cation formation has only been observed upon illumination of the radical with 400 nm light, i.e. upon excitation of the high energy $D_0 \rightarrow D_2$ band.

Finally, to unambiguously rule out the formation of solvated electrons via photodetachment from the radical, we have also carried out complementary pump-probe experiments on verdazyl dissolved in cyclohexane. In hydrocarbon solvents at room temperature, the solvated electron absorption band peaks in the mid-infrared spectral region around 2400 nm, i.e. shifted to lower photon energies by almost 3000 cm^{-1}.[64] Consistent with this enormous spectral shift, one can expect the absorbance of the solvated electron in cyclohexane solution to be much smaller than in acetonitrile solution. Consequently, the 720 nm-bleaching signal of the radical in cyclohexane solution should be much larger than in acetonitrile solution. However, the pump-probe data of the radical in the hydrocarbon solvent were found to be qualitatively very similar to those obtained in acetonitrile. In fact, the peak-to-peak ratio between the 720 nm-bleach and the 500 nm-absorption were found to be equal for these two solvents. This finding is clearly inconsistent with a relaxation mechanism that invokes an initial photodetachment of a solvated electron from the verdazyl radical and a subsequent recombination of the two ionization products.

4.6 Dark State Contributions and Signal Anisotropies

Having dismissed the photodetachment meachnism as a possible explanation for the apparent bleach deficiency, we must resort to additional absorptive electronic transitions of the type $D_0 \rightarrow D_n$, which can interfere with the $D_0 \rightarrow D_1$, bleaching signal. The TD-DFT calculations revealed additional electronically excited states (in particular, D_3 and D_4) that are energetically very close to D_2 but that carry almost negligible oscillator strength as compared

to D_1 and D_2. However, it could well be that, perhaps due to some kind of vibronic mixing [65], these states can couple radiatively to the ground state, when the latter is dressed with a significant amount of vibrational excitation; in particular, in those mode that can break the symmetry of the radical. Since this interpretation invokes the contribution of another absorptive resonance, $D_{0,hot} \rightarrow D_n$, in the spectral region of the bleach and because this spectroscopic activity depends on the internal energy of the radical, it can be tested in the following fashion.

The transient anisotropy, r(t), in a femtosecond pump-probe experiment is generally defined as the ratio between the anisotropic and isotropic signals, ΔOD_{aniso} and ΔOD_{iso}, respectively, according to

$$r(t) = \frac{\Delta OD_{aniso}(t)}{\Delta OD_{iso}(t)} = \frac{\Delta OD_{\parallel}(t) - \Delta OD_{\perp}(t)}{\Delta OD_{\parallel}(t) + 2\Delta OD_{\perp}(t)}, \quad (6)$$

where $\Delta OD_{\parallel}$ and $\Delta OD_{\perp}$ are the pump-induced optical densities that are measured with probe pulses polarized parallel and perpendicular with respect to the excitation pulse.[66] It can be shown that the anisotropy, r(0), at a time delay of zero is related to the angle, Ω(0), between the two transition dipole moments that are utilized in the sample's consecutive interactions with the pump and probe electric fields according to

$$r(0) = \frac{1}{5}\langle(3\cos^2\Omega(0) - 1)\rangle \quad (7)$$

where the angular brackets denote an ensemble average.[66] In the case of parallel pump and probe transition dipoles, Ω(0) is equal to zero and the polarization-resolved signals are related by $\Delta OD_{\perp}(0)/\Delta OD_{\parallel}(0) = 1/3$ such that the time-zero anisotropy becomes +2/5. In the case of orthogonal pump and probe transition dipoles, Ω(0) is equal to 90° and the polarization-resolved signals are connected by $\Delta OD_{\perp}(0)/\Delta OD_{\parallel}(0) = 2$ such that the time-zero anisotropy

becomes negative, i.e. r(0) = –1/5. Omitting from hereon the specific reference to time zero, we abbreviate the ratio between the two orthogonal signals by

$$R = \frac{\Delta OD_{\perp}}{\Delta OD_{\parallel}} = \frac{1-r}{1+2r}\,. \tag{8}$$

Equations (6) through (8) hold true regardless of whether the signal is absorptive (positive) or emissive (negative, such as a bleach).

Now suppose that the pump-probe signal is composed of two contributions, an induced bleach, ΔB, and an induced absorption, ΔA, such that we can write

$$\Delta OD_{iso} = \Delta B_{iso} + \Delta A_{iso}\,. \tag{9}$$

As above, we can express each component in terms of their individual polarization ratios and anisotropies

$$R_B = \frac{\Delta B_{\perp}}{\Delta B_{\parallel}} = \frac{1-r_B}{1+2r_B} \quad \text{and} \quad R_A = \frac{\Delta A_{\perp}}{\Delta A_{\parallel}} = \frac{1-r_A}{1+2r_A} \tag{10}$$

as well as in terms of their respective angles between pump and probe transition dipoles

$$r_B = \frac{1}{5}\langle(3\cos^2\Omega_B - 1)\rangle \quad \text{and} \quad r_A = \frac{1}{5}\langle(3\cos^2\Omega_A - 1)\rangle \tag{11}$$

From these relations, we can obtain an expression for the ratio of the two isotropic signal components, whose square root in turn, is proportional to the ratio of the magnitude of the two transition dipoles, μ_B and μ_A, that give rise to the induced bleach and induced absorption, respectively,

$$\frac{|\mu_A|}{|\mu_B|} = \sqrt{\frac{|\Delta A_{iso}|}{|\Delta B_{iso}|}} = \sqrt{\left|-\left(\frac{1+2R_A}{1+2R_B}\right)\left(\frac{R-R_B}{R-R_A}\right)\right|}\,. \tag{12}$$

Referring to the experimental pump-probe signals of verdazyl, the bleaching signal is the trivial component having parallel pump and probe transition dipoles and consequently, we

have $\Omega_B = 0$, $r_B = 2/5$, and $R_B = 1/3$. Provided an experimentally determined value of R (or equivalently, an experimental time-zero anisotropy, r) is available, one can use equation (12) to extract the relative magnitude of the transition dipole strength, $|\mu_A|$, of the additional absorptive component for any value of Ω_A ranging between 0 (when it is oriented parallel to the pump or bleach transition dipole) to 90° (when it is orthogonally oriented with respect to the pump or bleach transition dipole). The results of such calculations are shown in Figure 8 for various hypothetical values of R.

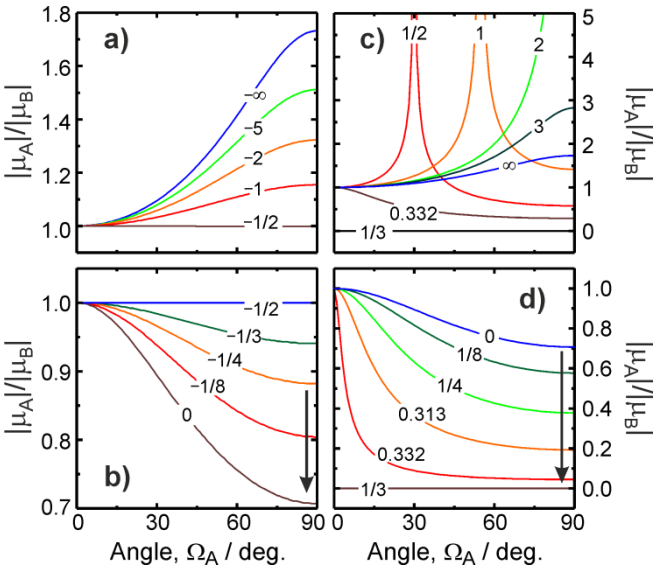

Fig. 8. Magnitude of absorption transition dipole relative to the bleaching (or equivalently, pump) transition dipole for various values of the perpendicular-to-parallel signal ratio, R, as indicated by the numbers. Since pump and bleach transition dipoles are inherently parallel, R_B was set to 1/3. The left column (a and b) corresponds to cases where parallel and perpendicular signals have opposite signs, whereas in right column (c and d), these two signals have the same sign.

In the limit where $\Omega_A = \Omega_B = 0$, the conditions $R = \Delta OD_{\perp}(0)/\Delta OD_{\parallel}(0) = 1/3$ holds generally true unless absorption and bleaching transition dipoles are equal, i.e. $|\mu_A|/|\mu_B| = 1$, in which case the pump-probe signal must vanish. In the limit where $\Omega_A = 0$ and $\Omega_B = 90°$,

the well-known condition, $R = \Delta OD_{\perp}(0)/\Delta OD_{\parallel}(0) = 2$ with $r = -1/5$, can be strictly fullfilled only if $|\mu_A|/|\mu_B| \rightarrow \infty$ (cf. panel c, R = 2) and a single resonance is detected. In general, the absorption-to-bleach transition dipole ratio can vary between 0 and ∞ depending upon the apparent ratio between the perpendicular and parallel signal strengths and their signs.[67] The situations typically encountered in pump-probe experiments are those depicted in panel c in which $1/3 \leq R \leq 2$ or equivalently, $2/5 \geq r \geq -1/5$. With the exception of R = 0, the traces considered in panels a and b entail situations, which are very rarely met in a pump-probe experiment; namely that the parallel and perpendicular pump-probe signals have opposite signs, e.g. $\Delta OD_{\parallel} < 0$ indicative of a net induced bleach and at the same time, $\Delta OD_{\perp} > 0$ signaling a net induced absorption. Finally, panel d includes situations in which the anisotropy exceeds the classical value of $2/5$. Here, the case of $R = 1/8$, which is equivalently to $r = 0.7$, should not be confused with a coherent preparation and simultaneous probing of two degenerate states having orthogonal transition dipoles as discussed by Galli et al. and others.[67-70]

We can now come back to clarifying the orgin of the bleach deficiency in the pump-probe data on triphenyverdazyl and our hypothesis of additional absorptive transitions to states that are dark when the radical is vibrationally cold, i.e. a resonance of the type $D_{0,hot} \rightarrow D_n$,. To this end, the parallel and perpendicular pump-probe signals and the resultant transient anisotropy at 720 nm, corresponding to the peak of the $D_0 \rightarrow D_1$ band, are studied in more detail. Remarkably, at early delays, the parallel trace displays a net bleach while the perpendicular trace displays a net absorption. According to our above discussion, this finding already demonstrates unambiguously that the 720 nm signal must indeed contain at least two transitions around t = 0. More quantitatively, the perpendicular-to-parallel signal ratio is $R = \Delta OD_{\perp}/\Delta OD_{\parallel} = \sim 5/(-20)$ corresponding to an initial anisotropy, r = 2.5. Therefore, these verdazyl data fall into the category sketched in panel b of Figure 8 with $R = -1/4$

from which we can conclude that the transition dipole of the additional $D_{0,hot} \rightarrow D_n$ absorption is about equal to the transition dipole of the $D_0 \rightarrow D_1$ absorption that is pumped at zero delay.

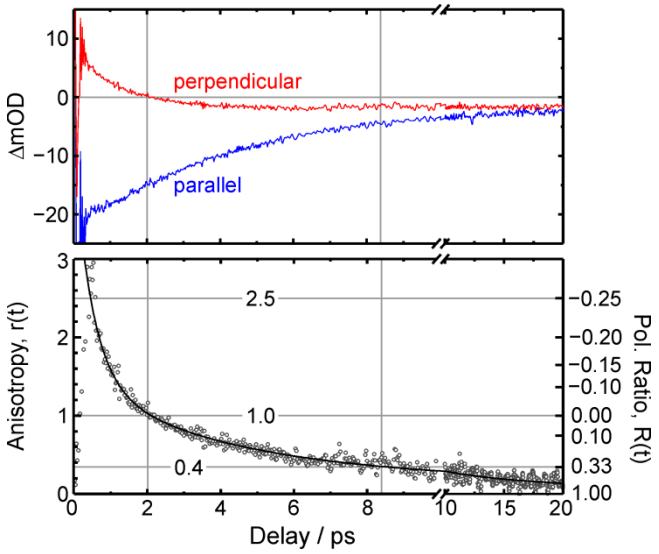

Fig. 9. Upper panel: Pump-probe kinetic traces measured with probe pulses whose polarization was parallel and perpendicular with respect to the pump pulses. Bottom panel: Resultant anisotropy calculated according to Equation (6). The solid curve is a fit to a multi-exponential decay.

In the following, we assume that $\Omega_B = 90°$, which gives a lower limit for the $D_{0,hot} \rightarrow D_n$ transition moment according to $|\mu_A|/|\mu_B| = 0.882$ (cf. Figure 8b), and we focus now on the temporal behavior of the polarization-resolved pump-probe traces shown in Figure 9. Whereas the parallel signal displays a continuous decay of the bleach, the perpendicular signal changes sign, being positive (absorptive) at early delays and emissive (bleach) at later delays. Apparently, the additional absorptive signal component decays so as to leave only a net bleach at late delays in both polarizations. In line with this notion, the transient anisotropy decays from its initial value of 2.5 asymptotically to the classical value of 0.4 within the first ten picoseconds. Subsequently, the anisotropy decays to zero on much longer time scales. Whereas the latter feature can be attributed to the overall rotational diffusion of the radical,

the initial decay of r(t) during the first 10 ps must be associated with the gradual decrease of the $D_{0,hot} \rightarrow D_n$ transition dipole strength as the molecule gradually vibrationally relaxes.

So long as the orientation of the transition moment for the $D_{0,hot} \rightarrow D_n$ resonance is stationary in the molecular frame of the radical, the vibrational relaxation dynamics can be depicted as a vertical downward-pointing arrow in the diagrams b and d of Figure 8. Immediately after photon absorption and internal conversion, the highly vibrationally excited radical is probed near 720 nm through the $D_0 \rightarrow D_1$ ground state bleach and the $D_{0,hot} \rightarrow D_n$ absorption. As a result of the high vibrational excitation these two signals have opposite sign but almost equal intensity. As the Franck-Condon active vibrations cool, the relative strength of $D_{0,hot} \rightarrow D_n$ absorption decreases so as to convert the D_n-state into the dark state that it was prior to optical excitation when the radical was cold. In this interpretation, the transient anisotropy formally calculated according to equation 6 reports on purely scalar dynamics, namely the dynamics of vibrational cooling, even though the transition moment vectors associated with the optical resonances of the radical do not rotate at all. This additional complexity buried in the apparent anisotropy due to overlapping transitions was also emphasized in an earlier publication by Unterreiner and coworkers.[67]

In a future publication, we will also attempt to extract the spectral dependence of the $D_{0,hot} \rightarrow D_n$ transition dipole moment at zero time delay. More importantly, we will also explore the photochemical primary events of 1,3,5-triphenyverdazyl following an excitation of its $D_0 \rightarrow D_2$ resonance in the near ultraviolet spectral region. Finally, having established that the excited state lifetime of verdazyl is ultrashort (< 1ps), we will engage in more sophisticated electronic structure calculations in an effort to identify any conical intersections between the D_1 and D_0 electronic states and the nuclear degrees of freedom that guide the molecular structure of the radical toward this critical configuration for the non-radiative decay. Inspired by complementary phenyl torsional dynamics in closed-shell organic systems

[71-72], we have initiated preliminary computational scans of the ground and first few excited-state potential energy surfaces along the two N–C $_{phenyl}$ and the C–C$_{phenyl}$ dihedral angles of triphenylverdazyl.

4. Conclusions

In summary, we have studied the ultrafast relaxation dynamics of 1,3,5-triphenyverdazyl radicals, a member of an intriguing class of thermodynamically stable organic radicals. The dynamics were explored in liquid solution using femtosecond pump-probe spectroscopy with 800 nm excitation. Following the absorption of the pump-photon, the initially prepared D_1-state of the radical relaxes non-radiatively to the electronic ground-states where it finds itself in high-lying vibrational states. The ensuing relaxation of vibrational energy leads to a characteristic spectro-temporal response in the visible spectral region, which we have analyzed within the framework of the Sulzer-Wieland formalism for describing the absorption spectra of hot polyatomic molecules. A characteristic bleach deficiency was noted in the near-infrared region of the $D_0 \rightarrow D_1$ transition, which was attributed to additional absorptive transitions from vibrationally excited states of D_0 to electronically excited states, D_n, which are in close energetic proximity to the D_2-state. At thermal equilibrium, the D_n-states are spectroscopically "dark", which is why their contribution to the pump-probe response fades away as the radical vibrationally relaxes. This interpretation was further scrutinized and corroborated by complementary transient anisotropy experiments, which revealed uncharacteristically high values around zero time delay. The anisotropy decay is consistent with vibrational relaxation and does not require the dynamic reorientation of the electronic transition dipole associated with the pump-probe signal in the near-infrared. Additional experiments are currently underway in our laboratories, which aim at exploring the primary

processes of verdazyl radicals following their $D_0 \rightarrow D_2$ electronic excitation in the near-ultraviolet spectral region.

Acknowledgements. Financial support by the Deutsche Forschungsgemeinschaft through the Collaborative Research Center, SFB 813, "Chemistry at Spin Centers" is gratefully acknowledged.

References

[1] L. J. Johnston, *Chem. Rev.* 1993, **93**, 251-266.

[2] I. Fischer, *Chemical Society Reviews* 2003, **32**, 59-69.

[3] T. Schultz, J. S. Clarke, T. Gilbert, H. J. Deyerl and I. Fischer, *Faraday Discuss.* 2000, **115**, 17-31.

[4] T. Schussler, W. Roth, T. Gerber, C. Alcaraz and I. Fischer, *Phys. Chem. Chem. Phys.* 2005, **7**, 819-825.

[5] B. Noller, R. Maksimenka, I. Fischer, M. Armone, B. Engels, C. Alcaraz, L. Poisson and J. M. Mestdagh, *J. Phys. Chem. A* 2007, **111**, 1771-1779.

[6] J. Herterich, T. Gerbich and I. Fischer, *ChemPhysChem* 2013, **14**, 3906-3908.

[7] Y. X. Huang and J. B. Hopkins, *J. Phys. Chem.* 1996, **100**, 9585-9591.

[8] D. Gosztola, M. P. Niemczyk, W. Svec, A. S. Lukas and M. R. Wasielewski, *J. Phys. Chem. A* 2000, **104**, 6545-6551.

[9] T. Häupl, R. Lomoth and L. Hammarström, *J. Phys. Chem. A* 2003, **107**, 435-438.

[10] L. Zhao, R. Lian, I. A. Shkrob, R. A. Crowell, S. Pommeret, E. L. Chronister, A. D. Liu and A. D. Trifunac, *J. Phys. Chem. A* 2004, **108**, 25-31.

[11] S. Amarie, U. Forster, N. Gildenhoff, A. Dreuw and J. Wachtveitl, *Chem. Phys.* 2010, **373**, 8-14.

[12] J. C. Gumy and E. Vauthey, *J. Phys. Chem. A* 1997, **101**, 8575-8580.

[13] S. Pages, B. Lang and E. Vauthey, *J. Phys. Chem. A* 2006, **110**, 7547-7553.

[14] M. Koch, A. Rosspeintner, K. Adamczyk, B. Lang, J. Dreyer, E. T. J. Nibbering and E. Vauthey, *J. Am. Chem. Soc.* 2013, **135**, 9843-9848.

[15] A. Rosspeintner, B. Lang and E. Vauthey, *Annu Rev Phys Chem* 2013, **64**, 247-271.

[16] A. Rosspeintner and E. Vauthey, *Phys. Chem. Chem. Phys.* 2014, **16**, 25741-25754.

[17] R. G. Hicks, John Wiley & Sons Ltd., Chichester, **2010**.

[18] R. Kuhn and H. Trischmann, *Mh. Chem.* 1964, **95**, 457-479.

[19] O. M. Polumbrik, *Russ. Chem. Rev.* 1978, **47**, 676-781.

[20] B. Pilawa, *Ann. Phys. (Leipzig)* 1999, **8**, 191-254.

[21] B. D. Koivisto and R. G. Hicks, *Coord. Chem. Rev.* 2005, **249**, 2612-2630.

[22] C. Train, L. Norel and M. Baumgarten, *Coord. Chem. Rev.* 2009, **253**, 2342-2351.

[23] G. N. Lipunova, T. G. Fedorchenko and O. N. Chupakhin, *Russ. Chem. Rev.* 2013, **82**, 701-734.

[24] C. Rullière, *Femtosecond Laser Pulses*, Springer Verlag, New York, **2003**.

[25] S. A. Kovalenko, A. L. Dobryakov, J. Ruthmann and N. P. Ernsting, *Phys. Rev. A* 1999, **59**, 2369-2384.

[26] A. R. Katritzky and S. A. Belyakov, *Synthesis-Stuttgart* 1997, 17-&.

[27] F. Neese, *Wires Comput. Mol. Sci.* 2012, **2**, 73-78.

[28] A. D. Becke, *Phys. Rev. A* 1988, **38**, 3098-3100.

[29] A. D. Becke, *J. Chem. Phys.* 1993, **98**, 5648-5652.

[30] C. T. Lee, W. T. Yang and R. G. Parr, *Phys. Rev. B* 1988, **37**, 785-789.

[31] A. Schäfer, H. Horn and R. Ahlrichs, *J. Chem. Phys.* 1992, **97**, 2571-2577.

[32] F. Weigend and R. Ahlrichs, *Phys. Chem. Chem. Phys.* 2005, **7**, 3297-3305.

[33] F. Neese, F. Wennmohs, A. Hansen and U. Becker, *Chem. Phys.* 2009, **356**, 98-109.

[34] F. Neese, *J. Comp. Chem.* 2003, **24**, 1740-1747.

[35] A. Klamt and G. Schüürmann, *J. Chem. Soc. Perkin Trans. 2* 1993, 799-805.

[36] S. Sinnecker, A. Rajendran, A. Klamt, M. Diedenhofen and F. Neese, *J. Phys. Chem. A* 2006, **110**, 2235-2245.

[37] A. Dreuw and M. Head-Gordon, *Chem. Rev.* 2005, **105**, 4009-4037.

[38] E. K. U. Gross, J. F. Dobson and M. Petersilka, in *Density Functional Theory II* (Ed.: R. F. Nalewajski), Springer Verlag, Berlin, **1996**.

[39] S. Hirata and M. Head-Gordon, *Chem. Phys. Lett.* 1999, **314**, 291-299.

[40] F. Neese and G. Olbrich, *Chem. Phys. Lett.* 2002, **362**, 170-178.

[41] T. Petrenko, S. Kossmann and F. Neese, *J. Chem. Phys.* 2011, **134**, 054116

[42] S. Grimme, *J. Chem. Phys.* 2006, **124**, 034108

[43] S. Grimme and F. Neese, *J. Chem. Phys.* 2007, **127**, 154116

[44] P. O. Löwdin, *J. Chem. Phys.* 1950, **18**, 365-375.

[45] P. O. Löwdin, in *Advances in quantum chemistry, Vol. 5* (Ed.: P. O. Löwdin), Academic Press Inc., New York, **1970**, pp. 185-199.

[46] D. E. Williams, *J. Am. Chem. Soc.* 1969, **91**, 1243-&.

[47] D. E. Williams, *Acta Crystallogr. B* 1973, **B 29**, 96-102.

[48] P. H. H. Fischer, *Tetrahedron* 1967, **23**, 1939-&.

[49] D. E. Berry, R. G. Hicks and J. B. Gilroy, *J. Chem. Ed.* 2009, **86**, 76-79.

[50] S. Mukamel, *Principles of nonlinear optical spectroscopy*, Oxford University Press, New York, **1995**.

[51] P. Sulzer and K. Wieland, *Helv. Phys. Acta* 1952, **25**, 653-676.

[52] D. C. Astholz, L. Brouwer and J. Troe, *Ber. Bunsenges. Phys. Chem.* 1981, **85**, 559-564.

[53] O. Schalk, J. P. Yang, A. Hertwig, H. Hippler and A. N. Unterreiner, *Mol. Phys.* 2009, **107**, 2159-2167.

[54] S. C. Doan and B. J. Schwartz, *J. Phys. Chem. Lett.* 2013, **4**, 1471-1476.

[55] S. C. Doan and B. J. Schwartz, *J. Phys. Chem. B* 2013, **117**, 4216-4221.

[56] J. Urbanek, A. Dahmen, J. Torres-Alacan, P. Königshoven, J. Lindner and P. Vöhringer, *J. Phys. Chem. B* 2012, **116**, 2223-2233.

[57] J. Urbanek and P. Vohringer, *J. Phys. Chem. B* 2014, **118**, 265-277.

[58] J. Urbanek and P. Vöhringer, *J. Phys. Chem. B* 2013, **117**, 8844-8854.

[59] S. Kratz, J. Torres-Alacan, J. Urbanek, J. Lindner and P. Vöhringer, *Phys. Chem. Chem. Phys.* 2010, **12**, 12169-12176.

[60] X. Y. Chen and S. E. Bradforth, *Annu. Rev. Phys. Chem.* 2008, **59**, 203-231.

[61] A. R. Katritzky and S. A. Belyakov, *Synthesis* 1997, 17-19.

[62] N. F. Guba, L. N. Ganyuk and V. D. Pokhodenko, *Theoret. Exp. Chem.* 1981, **17**, 254-258.

[63] R. Kuhn, F. A. Neugebauer and H. Trischmann, *Mh. Chem.* 1966, **97**, 1280-1289.

[64] L. Kevan, H. A. Gillis, K. Fueki and T. Kimura, *J. Chem. Phys.* 1978, **68**, 5203-5205.

[65] T. Azumi and K. Matsuzaki, *Photochem. Photobiol.* 1977, **25**, 315-326.

[66] G. R. Fleming, *Chemical applications of ultrafast spectroscopy*, Oxford University Press, New York, **1986**.

[67] Y. Liang, M. Klinger, O. Schalk and A. N. Unterreiner, *J. Chem. Phys.* 2013, **139**, 224309

[68] C. Galli, K. Wynne, S. M. LeCours, M. J. Therien and R. M. Hochstrasser, *Chem. Phys. Lett.* 1993, **206**, 493-499.

[69] S. Hess, H. Bürsing and P. Vöhringer, *J. Chem. Phys.* 1999, **111**, 5461-5473.

[70] O. Schalk and A. N. Unterreiner, *Z. Phys. Chem.* 2011, **225**, 927-938.

[71] J. Schroeder, J. Troe and P. Vöhringer, *Z. Phys. Chem.* 1995, **188**, 287-306.

[72] J. Schroeder, D. Schwarzer, J. Troe and P. Vöhringer, *Chem. Phys. Lett.* 1994, **218**, 43-50.